Structural investigation of xenon-ion-beam-irradiated glassy carbon

D. G. McCulloch*
Department of Materials Engineering, Monash University, Clayton, Victoria 3168, Australia

S. Prawer
School of Physics, Micro Analytical Research Centre, University of Melbourne, Parkville, Victoria 3052, Australia

A. Hoffman
Chemistry Department, Technion Israel Institute of Technology, Haifa 32000, Israel
(Received 2 December 1993; revised manuscript received 4 May 1994)

Raman spectroscopy, cross-sectional transmission electron microscopy, and electron-energy-loss spectroscopy have been used to monitor the ion-beam-induced transformation in glassy carbon irradiated with 320-keV Xe ions to doses between 5×10^{12} and 6×10^{16} ions/cm^2. It was found that (i) the ion beam amorphizes the glassy carbon structure; (ii) the amorphization is accompanied by a compaction of the glassy carbon from an initial density of 1.55 to 2.2 ± 0.2 g/cm^3; and (iii) approximately 15% of the graphitelike bonds in glassy carbon are converted to diamondlike bonds in the amorphization process. The transformation of glassy carbon to an amorphous state occurs in two distinct stages as a function of ion dose. For damage levels up to 0.2 displacements per atom (dpa) the effect of the ion beam is to decrease the average graphitic crystallite size. Above 0.2 dpa, disorder in bond length and bond angle away from ideal graphitic threefold coordination occurs leading to complete amorphization at high doses. The amorphization, compaction, and presence of $\approx15\%$ sp^3 bonds in the implanted layer of glassy carbon results in a surface layer which is significantly more resistant to abrasion than as-grown glassy carbon.

I. INTRODUCTION

A. Glassy carbon

Synthetic graphites are an important class of materials which, because of their chemical inertness and high electrical conductivity, have a wide range of industrial applications as materials for use in electrodes, crucibles, and biomaterials.[1,2] Glassy carbon (GC) is one example of a synthetic graphite produced by the decomposition of highly cross-linked polymers. The structure and properties of GC depend on the heat treatment temperature during manufacture. X-ray diffraction experiments have revealed that GC consists of carbon atoms bonded predominantly in graphitelike planes. The registry between these graphitic planes is, however, poor. Examination of GC in the transmission electron microscope (TEM) reveals a structure comprised of tangled graphitelike ribbons. The size of these ribbonlike stacks for GC heat treated to 2500 °C is estimated to be up to 10 nm long and 4 nm in cross section. The tangled graphitic microstructure of GC is resistant to three-dimensional ordering even when heat treated to temperatures in excess of 3000 °C. For this reason, GC is classified as a nongraphitizing carbon.[2]

Ion implantation is a technique which can produce metastable layers in materials via nonequilibrium processes.[3] In addition to providing a mechanism for the introduction of foreign species into a host material, ion implantation can be employed to reproducibly and controllably alter the level of disorder within the host structure, potentially leading to desirable changes in the surface properties of materials. In particular, ion-beam irradiation has been shown to significantly enhance the abrasive wear resistance of GC.[4,5] It has been shown that the ion-beam-induced wear resistance is independent of the implanted ion species, suggesting that the hardening process is damage driven and not due to chemical effects.[6] However, whilst the implantation conditions under which GC becomes resistant to wear are well characterized, the mechanisms behind this toughening are not well understood. An understanding of the mechanisms behind this increase in wear resistance is one of the goals of the present study. In addition, this study seeks to further elucidate the effects of ion implantation on the structure of graphitic materials. Since the structure and properties of GC are well documented, GC is an ideal prototype material for such a study. The present work is concerned with the structural changes which occur to GC as it is transformed from a predominantly graphiticlike structure to an essentially amorphous state under the action of the ion beam.

In order to investigate ion-beam-induced damage effects, GC substrates were irradiated with xenon ions to doses between 5×10^{12} and 6×10^{16} ions/cm^2. Xenon ions are ideal for ion-beam-induced damage studies of GC, since they create a large damage density in the carbon matrix while, at the same time, they are unlikely to be chemically active, with the possible exception of causing the formation of inert gas bubbles at doses in excess of $\approx10^{16}$ Xe/cm^2.[7] Thus for doses below 10^{16} Xe/cm^2 changes in the structure of GC are predominantly due to the introduction of damage.

B. Techniques of analysis

Due to its sensitivity to structural changes, Raman spectroscopy has proved to be a powerful technique for monitoring changes in the microstructure of various carbon-based materials.[8] For example, Raman spectroscopy has been used to help understand changes in the microstructure of graphite and diamond following ion irradiation.[1] The first-order Raman spectrum of graphite consists of one peak at 1582 cm^{-1} (the G peak) attributable to in-plane symmetric C-C stretching (E_{2g}). The first-order Raman spectrum of GC is dominated by two peaks. The first is at ≈ 1590 cm^{-1} (the G peak), originating from lattice vibrations in the plane of the graphitelike ribbons present in the GC structure. The second peak is the so-called disorder or D peak at ≈ 1355 cm^{-1} which occurs in graphitic materials with small crystallite sizes. Also present in the Raman spectrum of GC is a small peak at 1615 cm^{-1} (the D' peak) which appears as a high-wave-number shoulder on the G peak. Since the G and D' peaks are usually unresolved from one another, the presence of the D' peak can lead to a higher than expected apparent G peak position in GC. The D and D' peaks correspond to local maxima in the phonon density of states (DOS) of graphite.[9] Normally, the $k=0$ selection rule restricts the observed phonons to those near the Brillouin zone center and hence the D and D' peaks are not observed in the Raman spectrum. However, as the level of disorder increases and long-range translational symmetry is lost, the $k=0$ selection rule is relaxed and phonons with non-zero k vectors throughout the Brillouin zone may contribute to the Raman spectrum.

It has been shown that ion implantation of GC tends to broaden these peaks and eventually produces a broad asymmetric peak near 1550 cm^{-1} similar to that obtained from amorphous carbon (a-C).[10] By examining the change in the G and D peak positions and widths as a function of ion dose, it was found that the transformation begins to occur at a damage level of 0.21 displacements per atom (dpa) for a wide range of ion species (H, He, C, N, Si, and Xe).[11]

The Raman spectra in the present study have been collected from Xe-irradiated GC with a vastly better signal-to-noise ratio than the spectra published in the previous investigation.[11] Despite past success in fitting the Raman spectrum of implanted GC with two Lorentzians, it was found that a superior fit was achieved by fitting a Lorentzian line near ≈ 1350 cm^{-1} and an asymmetric Breit-Wigner-Fano (BWF) line shape at ≈ 1600 cm^{-1}. Dillon, Woollam, and Katkanant[12] also found that asymmetric line shapes provided superior fits to the Raman spectra of annealed a-C films than those obtained using symmetric Lorentzians. It was suggested that an asymmetric line shape fits the Raman spectrum of disordered carbon better than a symmetric line shape due to the asymmetric nature of the DOS curve for graphite in the region of the D and G lines. The BWF line shape arises in Raman scattering as a result of the interaction between discrete Raman-active phonon modes and a continuum of Raman-active modes.[13] The BWF line shape has been observed in implanted graphite[14,15] and stage-1 alkali-metal graphite intercalation compounds.[16] In graphite-based materials the interaction is thought to be between the zone center E_{2g} mode and a broad continuum of modes which becomes active as the $k=0$ selection rule breaks down. The origin of the broad continuum which gives rise to the BWF line shape has been attributed to a disorder-induced phonon mechanism.[16]

The cross-sectional TEM specimens of implanted GC were prepared using ultramicrotomy. Ultramicrotomy has proved to be a successful technique for slicing sections of GC which are sufficiently thin to be able to be readily observed in the TEM.[18,19] By viewing the implanted GC samples in cross section, the depth of the implanted layer can be accurately determined. In addition, large areas of specimen with uniform thickness can be produced which are ideal for the application of electron-energy-loss spectroscopy (EELS). EELS is a powerful technique for investigating carbon-based materials since it can be used to estimate the fraction of diamondlike (sp^3) to graphitelike (sp^2) bonding present.[20]

In a recent investigation[18] it was shown that ion implantation of GC with 50-keV C ions to a dose of 5×10^{16} C/cm^2 leads to an increase in density of the implanted layer from 1.55 to 2.4 ± 0.2 g/cm^3. In that study the density of the implanted layer was determined from measurements of the depth of the implanted layer obtained from cross-sectional TEM images and measurements of the step height between unimplanted and implanted areas of the sample. Concomitant with this increase in density is an observed increase in refractive index from 1.8 to 2.4 ± 0.1. The increase in refractive index was attributed to an increase in electron density of the denser implanted layer. It has been suggested[18] that the increase in density of the implanted layer is an important factor to consider in attempting to understand the transformation of GC under the influence of an ion beam. In the present study, ellipsometry and step-height measurements are employed to monitor the dose dependence of changes in the density of the implanted layer.

Collectively, these diagnostics provide an insight into the nature of the ion-beam-induced transformation in GC and may be used to suggest a model for the increase in wear resistance of the material following ion implantation.

II. EXPERIMENT

A. Ion implantation

The GC substrates were cut from plates supplied by Atomergic Chemetals Corporation (New York). According to the manufacturer's specifications, the GC was heat treated to 2500 °C and has a density of 1.5–1.55 g/cm^3. Prior to implantation the GC substrates were polished with progressively finer diamond paste down to a 1-μm finish on a cloth lap. The samples were then mounted onto a Cu target holder using Ag paste and implanted with 320-keV Xe ions to doses between 5×10^{12} and 6×10^{16} ions/cm^2 in a vacuum better than 1×10^{-5} Torr. Beam currents were kept below 1 $\mu A/cm^2$ to minimize beam heating of the sample during the irradiation. The range (R_p) and straggling (ΔR_p) of 320-keV Xe ions in

GC were calculated by the TRIM computer program[21] to be 130 and 20 nm, respectively. Thus the implanted layer is expected to have a thickness of ≈ 150 nm ($R_p + \Delta R_p$).

B. Raman spectroscopy

The Raman spectra were taken in a near-backscattering geometry on a Dilor Microdil 28 micro-raman spectrometer with an Ar ion laser operating at 488 nm. The laser was focused down to a 2-μm spot with a 50× objective lens and a laser power of 100 mW was employed. The spectra were taken over the range 1000–1800 cm^{-1} with a resolution of 5 cm^{-1}. In order to test whether the laser used for the Raman measurement was modifying the implanted specimens at a power of 100 mW, Raman spectra were also taken with reduced powers down to 40 mW. No change in the Raman spectrum was observed upon decreasing the laser power and hence a laser power of 100 mW was used for all the measurements presented here. The skin depth of the laser light in disordered carbons is 80–100 nm.[15] In order to check the possibility that the incident laser light penetrates the ion-beam-implanted layer and samples the underlying unimplanted GC, Raman spectra were obtained from some of the implanted samples with the laser beam incident at 60° from the surface normal. The resulting spectra were identical to those obtained in the near-backscattering geometry, indicating that the underlying unimplanted substrate contributes little to the Raman spectrum.

In order to analyze the Raman spectra quantitatively, the Raman spectra were fitted with a BWF G peak, Lorentzian D peak, and a linear background using a linear least-squares computer program. The BWF line shape is described by the following expression:

$$I(\omega)=\frac{I_0[1+2(\omega-\omega_0)/q\Gamma]^2}{1+[2(\omega-\omega_0)/\Gamma]^2} . \quad (1)$$

In Eq. (1), $I(\omega)$ is the intensity as a function of frequency, I_0 is the peak intensity, ω_0 and Γ are the peak position and full width at half maximum (FWHM), respectively, and q^{-1} is the Breit-Wigner-Fano coupling coefficient. In the limit $q^{-1}\rightarrow 0$, the Lorentzian line shape is recovered. In annealing studies of implanted graphite the limit of $\Gamma/q\rightarrow 0$ has been identified as the point where in-plane ordering is complete and three-dimensional ordering begins.[15] Thus Γ/q (the coupling parameter) can be used as a measure of in-plane graphic order.

C. Cross-section transmission electron microscopy

In order to prepare cross-sectional TEM specimens a sliver of each implanted GC specimen was embedded into a hard epoxy resin (Epon 812 equivalent) and then cross-sectional sections cut using a diamond knife in an ultra microtome.[22] The thickness of the thin sections were estimated to be less than 60 nm from the interference colors observed in the sections while cutting. Cutting speeds of 0.2–0.5 mm/s were found to produce the best sections. The TEM was performed using a JEOL 2010 electron microscope operating at 200 keV. The Rayleigh resolution of this electron microscope is approximately 0.23 nm at the Schertzer defocus condition. The selected area diffraction patterns were taken from an area of the sample with a diameter of 100 nm using the smallest selected area diffraction aperture available on the microscope.

D. Electron-energy-loss spectroscopy

The EEL spectra were taken using a Gatan 666 Parallel EEL spectrometer, fitted beneath a Philips CM20 transmission electron microscope operating at 80 keV. All spectra were taken with the microscope in scanning mode with an electron probe convergence semiangle on the specimen of 8 mrad. The electron beam was estimated to illuminate an area of the sample with a diameter of ≈ 5 nm. The spectra were collected with a spectrometer acceptance semiangle of 4 mrad. The energy resolution of the spectrometer, as measured by the full width at half maximum of the zero-loss peak, was 1.2 eV.

E. Ellipsometry

The refractive index of the implanted samples was measured using an ellipsometer equipped with a He-Ne laser. The Fresnel equation for a one-interface system (i.e., air/implanted GC) was employed.[23] Analysis requiring a two-interface model (i.e., air/implanted GC/unimplanted GC) was not necessary since, as discussed above, the skin depth of the laser light is expected to be less than the thickness of the implanted layer, especially since these measurements were carried out at a glancing angle of 70° to the surface normal.

III. RESULTS AND DISCUSSION

A. Raman spectroscopy

The Raman spectra of GC samples irradiated at room temperature with increasing doses of 320-keV Xe ions are shown in Fig. 1. Also shown in the figure are the fits to the data using the BWF-Lorentzian line-shape combination. As the dose increases, the general trend apparent in Fig. 1 is that the D and G peaks broaden as a result of an increase in disorder in the system. As the G peak broadens, the G and D' peaks become unresolved from one another. For the sake of simplicity, the more energetic peak will continue to be referred to as the G peak.

The G and D peak parameters extracted from the fits to the data in Fig. 1 are plotted as a function of Xe dose in Figs. 2–5 below. In order to compare damage produced by different ions in a solid it is often convenient to calculate the number of displacements per atom (dpa) for a given ion dose. The top axis in the plots shown in Figs. 2–5 displays the number of dpa corresponding to each dose calculated by dividing the average vacancy concentration calculated using TRIM (Ref. 21) by the atomic density of GC.[11] Essentially, the dpa parameter is proportional to the energy density deposited by the incoming ion in nuclear collisions. Because TRIM does not take into account dynamic annealing or the effect of multiple impacts, the dpa parameter almost certainly overestimates the actual damage density for a given ion dose.

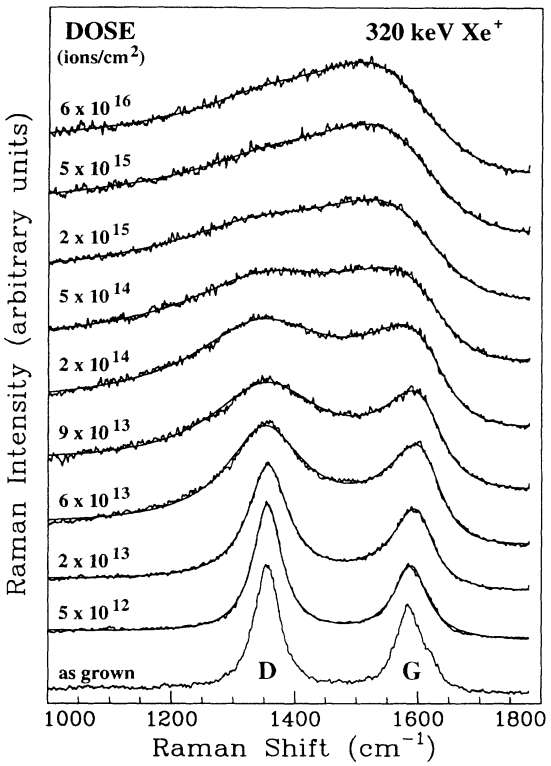

FIG. 1. Raman spectra of glassy carbon samples irradiated at room temperature with increasing doses of 320-keV Xe^+ ions. The implanted samples have been fitted with one Lorentzian line shape for the *D* or disorder peak and one Breit-Wigner-Fano line shape for the *G* or graphite peak using a least-squares algorithm.

The error bars in Figs. 2–5 are indicative of the spread of values obtained by collecting Raman spectra from different regions on a particular implanted sample and then fitting each spectrum using the procedure outlined above. At higher ion doses or dpa, the *G* peak begins to dominate the overall fit, $I(D)$ becomes very small, and so there is generally a larger spread of values associated with the *D* peak parameters than the *G* peak parameters.

In order to help understand the connection between changes in the Raman spectrum and structural changes which occur in GC following ion bombardment, reference will be made to the work of Beeman *et al.*[17] Beeman and his colleagues calculated the vibrational DOS and corresponding Raman spectrum for various model structures of disordered carbon using the equation of motion method. For a graphite structure with ideal 120° threefold-coordinated bonding, the Raman spectrum calculated by Beeman was found to display peaks at 1591 and 1310 cm^{-1} which were identified as the *G* and *D* peaks experimentally observed in microcrystalline graphite. As the average bond angle in the model structure was changed from the ideal graphitelike 120° due to introduction of five- and sevenfold membered rings, the peak at ≈ 1600 cm^{-1} in the calculated Raman spectrum shifted down in frequency, while the *D* peak remained unchanged. This result suggested that a deviation in the average bond angle in a purely threefold-coordinated material can lead to a decrease in *G* peak position with little change in the *D* peak position. In addition to model structures consisting of purely threefold-coordinate bonding, Beeman *et al.* also studied the effect on the DOS and Raman spectrum of model structures containing different percentages of diamondlike fourfold-coordinated bonding. It was found that, as the percentage of fourfold-coordinated bonds increased, a decrease in both the *G* and *D* peaks is observed. This latter result suggests that a simultaneous downward shift in both the *G* and *D* peaks of a disordered carbon may be indicative of the presence of fourfold-coordinate bonding.

Figures 2(a) and 2(b) show the position (ω_0) and

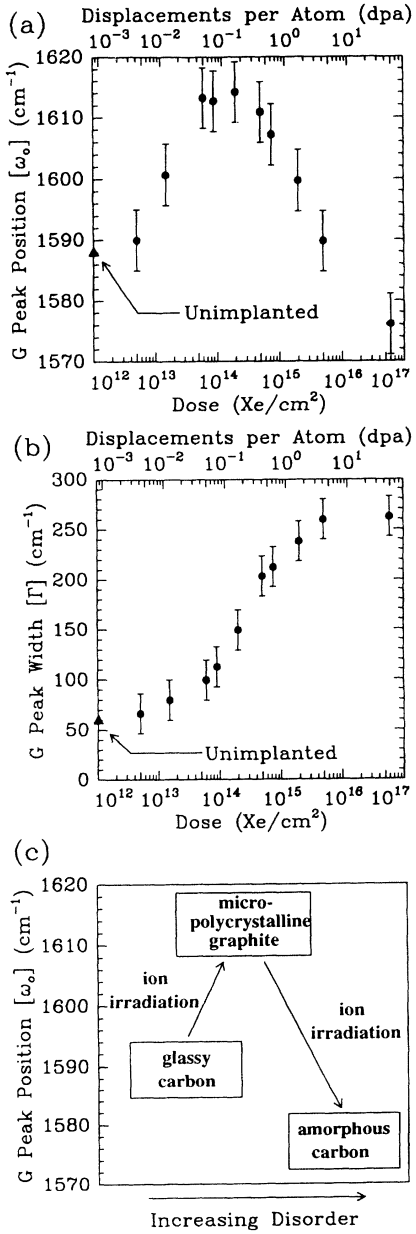

FIG. 2. The (a) position (ω_0) and (b) FWHM (Γ) of the Breit-Wigner-Fano *G* peak plotted against Xe dose. The ▲ on the ordinate axis indicates the values of ω_0 and Γ for the unirradiated glassy carbon. The schematic in (c) shows how the changes in *G* peak position correspond to changes in the glassy carbon structure following ion irradiation (see text).

FWHM (Γ) of the BWF G peak as a function of Xe ion dose. At a dose of 5×10^{12} Xe/cm^2, $\omega_0\approx1590$ cm^{-1}, which is close to the value obtained for the G peak position of unirradiated GC of ≈1588 cm^{-1}. As the Xe dose increases above 5×10^{12} Xe/cm^2, there is an increase in ω_0, which reaches a maximum value of ≈1615 cm^{-1} for doses between 6×10^{13} and 2×10^{14} Xe/cm^2 before decreasing again. The shift in the position of the BWF line from 1588 to 1615 cm^{-1} can be understood with reference to the phonon dispersion curve for graphite.[9] As the ion dose is increased and the GC structure becomes more damaged, a decrease in the average graphitic crystalline size allows k vectors away from the zone center to contribute to the Raman spectrum, resulting in an increase in the contribution to the Raman spectrum of the 1615-cm^{-1} peak in the DOS.[9] The increased contribution in this portion of the DOS leads to an apparent shift in the G peak position from ≈1588 to ≈1615 cm^{-1}. This interpretation for the upward shift in the G peak position in terms of an increased contribution of the D' peak at 1615 cm^{-1} is supported by calculations carried out by Lespade, Al-Jishi, and Dresselhaus.[24] They studied the effects of decreasing the size of two-dimensional graphitic crystallites on the Raman spectrum and found that, indeed, as the average graphite particle size decreased, the D' peak increased in intensity with respect to the G peak.

Between doses of 6×10^{13} and 2×10^{14} Xe/cm^2 the G peak position stays relatively constant at ≈1615 cm^{-1}. A G peak value of 1615 cm^{-1} in this dose range indicates that the irradiated material still contains a large proportion of graphitelike threefold-coordinate bonding as indicated by the continued agreement with the phonon DOS of graphite. Figure 2(c) diagrammatically shows the expected shifts in the Raman line which should accompany the transformation between GC and a material which contains small crystallites of graphite (micropolycrystalline graphite) for doses between 5×10^{12} and 6×10^{13} Xe/cm^2.

For Xe doses exceeding $\approx2\times10^{14}$ ions/cm^2 or 0.2 dpa, the BWF line position shows a monotonic decrease from ≈1615 to ≈1575 cm^{-1}. As discussed above, modeling studies by Beeman and his colleagues[17] have shown that a change in the bond angle away from the ideal 120° results in a decrease in the frequency of the G peak. Therefore the decrease in G peak position observed in the Raman spectrum at higher doses indicates that the level of disorder has increased sufficiently to alter the average bond angle within the implanted layer away from 120°. The reverse of this process was observed by Dillon, Woollam, and Katkanant[12] who noted an increase in the G peak position as the proportion of graphitelike bonding within their a-C films increased by thermal annealing. A second possibility that some of the decrease in G peak position is due to the presence of fourfold-coordinate bonding will be discussed below. What is clear is that the downward shift in the G peak position at damage levels above ≈0.2 dpa indicates that the phonon density of states of graphite no longer well describes the implanted layer in GC and thus this downward shift can be interpreted as evidence for a transformation from micropolycrystalline graphite into a-C as shown schematically in Fig. 2(c).

The FWHM of the G peak [Fig. 2(b)] shows a dramatic broadening from ≈60 cm^{-1} at low doses to ≈260 cm^{-1} for Xe doses above 2×10^{15} Xe/cm^2. A broadening of the G peak can be interpreted as an increase in bond-angle disorder. The initial increase in G peak width probably corresponds to the introduction of point defects such as C interstitials and vacancies within the graphitelike planes.[8] The greatest rate of increase in the G peak width occurs at a damage level of ≈0.2 dpa, corresponding to the point where the average bond angle changes from the ideal graphitelike 120° as the material transforms from a micropolycrystalline graphite to an a-C. Eventually, at a damage level of 4 dpa the G peak FWHM saturates, which probably indicates that the damage level has also saturated and the structure has completely amorphized. However, the downward shift in the G peak position at damage levels in excess of 4 dpa suggests that, although the implanted layer has amorphized, the ion beam continues to reduce the average bond angle within the amorphous irradiated material.

Figure 3(a) shows the Breit-Wigner-Fano coupling parameter Γ/q plotted as a function of Xe ion dose. As discussed above, the limit of $\Gamma/q\rightarrow0$ has been identified as

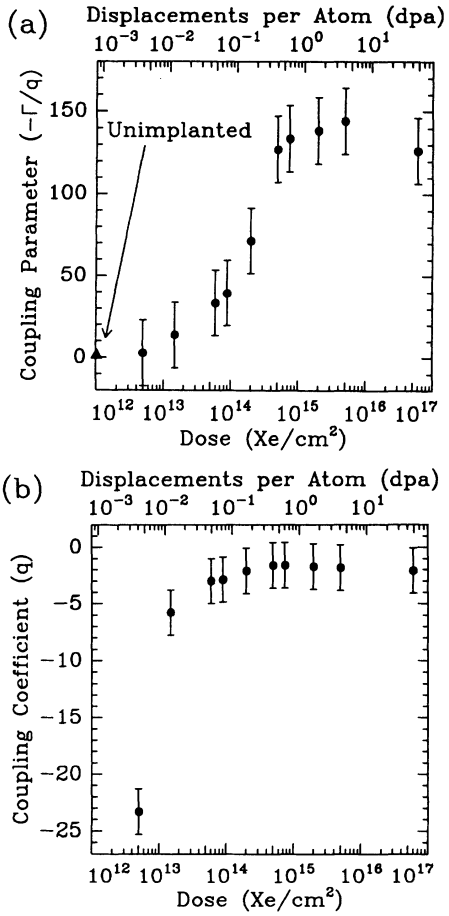

FIG. 3. The (a) coupling parameter (Γ/q) and (b) coupling coefficient (q) for the Breit-Wigner-Fano line shape used to fit the G peak plotted against Xe dose. The ▲ on the ordinate axis indicates the coupling parameter for unirradiated glassy carbon in (a). The coupling coefficient for unirradiated glassy carbon is off scale at ≈-300.

the point where in-plane graphitic ordering is complete and three-dimensional ordering begins.[15] Thus the Γ/q parameter can be used as a measure of in-plane graphitic order. The coupling parameter for unimplanted GC approaches 0, supporting the proposition that excellent in-plane ordering exists in GC as indicated by its radial distribution function.[25] It can be seen from the figure that there is a significant increase in the magnitude of the coupling parameter for Xe doses up to $\approx 10^{15}$ Xe/cm^2. Above this dose a saturation of Γ/q is observed. In Fig. 3(b) the coupling coefficient q is plotted as a function of Xe dose. The large increase in q for damage levels up to $\approx 10^{14}$ Xe/cm^2 indicates that the coupling factor is very sensitive to damage at low doses as the G peak changes from a crystalline symmetric line shape to the BWF line shape. Above doses of $\approx 10^{14}$ Xe/cm^2 q saturates. Thus the trend in Γ/q for doses above $\approx 10^{14}$ Xe/cm^2 is dominated by the FWHM (Γ) and the coupling parameter (Γ/q) versus dose curve closely resembles the FWHM (Γ) versus dose curve shown in Fig. 2(b). The dose dependence of the coupling parameter indicates that there is a substantial structural change occurring at a dose of $\approx 2\times 10^{14}$ Xe/cm^2 (0.2 dpa) since at this point it rises sharply. A damage density of 0.2 dpa corresponds to the production of approximately one vacancy per C hexagon in the graphitic ribbons which make up GC. Thus 0.2 dpa corresponds to the point where the graphitic bonding within the GC structure begins to break up.

In Fig. 4 the relative intensity of the D and G peaks [the $I(D)/I(G)$ ratio] is plotted against Xe dose. It has been shown that the $I(D)/I(G)$ ratio is inversely proportional to the in-plane crystalline size (L_a) for disordered graphite.[26] Recently it was shown that this relationship holds for a wide range of sp^2-bonded carbons over the range $2.5 < L_a < 300$ nm for laser wavelengths of 488 and 514.5 nm.[8] Using the calibration curves provided in these previous investigations, it is estimated that an $I(D)/I(G)$ ratio of 1.2 which is observed for unirradiated GC corresponds to an L_a of ≈ 3.5 nm. It can be seen from the figure that there is an initial increase in the $I(D)/I(G)$ ratio between unimplanted GC and the sample implanted at the lowest dose (5×10^{12} Xe/cm^2). This initial increase in the $I(D)/I(G)$ ratio probably corresponds to a decrease in the in-plane crystallite size as the ion implantation introduces disorder into the system. For implantation doses above 5×10^{12} Xe/cm^2 the $I(D)/I(G)$ ratio decreases linearly. This downward trend in the $I(D)/I(G)$ ratio with increasing Xe dose cannot be interpreted as an increase in crystalline size as would be predicted be an application of the relationship $1/L_a \alpha I(D)/I(G)$. However, since L_a of unimplanted GC is near the lower limit for the validity of the above relationship, it is not surprising that $I(D)/I(G)$ cannot be effectively used to estimate crystallite size in irradiated GC.

A possible explanation for the decrease in $I(D)/I(D)$ with increasing dose is as follows. As discussed above, the D peak originates from the peak in the density of states of graphite at points $k\neq 0$ in the Brillouin zone. However, as the damage level is increased and the implanted material suffers a loss of short-range order, the

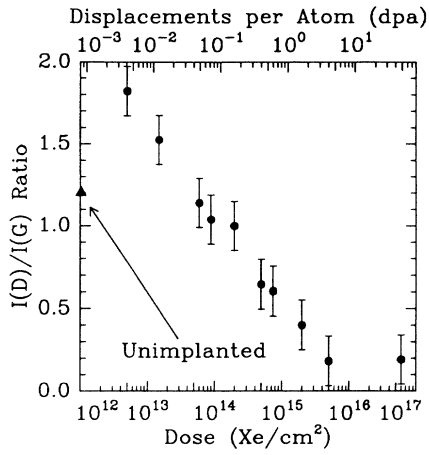

FIG. 4. $I(D)/I(G)$ ratio plotted as a function of Xe dose. The ▲ on the ordinate axis indicates the value of $I(D)/I(G)$ for unirradiated glassy carbon.

DOS of graphite can no longer be directly applied to this system. It has been shown from modeling studies of highly disordered carbons that the DOS consists of a single broad asymmetric peak.[17] Thus for graphitic materials an increase in the intensity of the D peak indicates a decrease in crystallite size. By contrast, for highly disordered graphites, with $L_a < 2.5$ nm, a decrease in the D peak intensity at high damage levels may represent a further increase in disorder as the system transforms from a microcrystalline graphite to a-C.

In Figs. 5(a) and 5(b) the position (ω_0) and FWHM (Γ) of the Lorentzian D peak are shown as a function of ion dose. Above doses of $\approx 10^{15}$ Xe/cm^2 the D peak becomes small compared to the G peak as indicated by the low value of the $I(D)/I(G)$ ratio, and the peak-fitting program has difficulty determining the D peak parameters of position and FWHM. In this dose regime it is in fact possible to obtain an adequate fit to the data with a single BWF line (i.e., $I(D)=0$]. Hence trends in the D peak parameters can only be followed reliably for Xe doses up to $\approx 10^{15}$ Xe/cm^2. Despite this limitation there are some trends apparent in both the D peak position and width. There is some evidence for a slight decrease in the D peak position from ≈ 1355 to ≈ 1345 cm^{-1}. As discussed above, modeling studies by Beeman and his colleagues[17] have shown that a simultaneous decrease in both the D and G peak frequencies may indicate the presence of some fourfold-coordinated bonds. Thus at high Xe doses, as the GC structure becomes highly disordered, there is the possibility that a small percentage of carbon atoms present within the implanted layer are tetragonally bonded. Given the errors in the position of the D peak evident in the Raman data, this possibility would remain purely speculative. However, in Sec. III C it is shown using EELS that the implanted layer in GC does indeed contain a small percentage of diamondlike bonds.

The D peak width shows a clear dependence on dose with a change from ≈ 75 cm^{-1} at low doses to ≈ 300 cm^{-1} at a dose of $\approx 10^{15}$ Xe/cm^2. This trend in the D peak FWHM is similar to that shown by the G peak

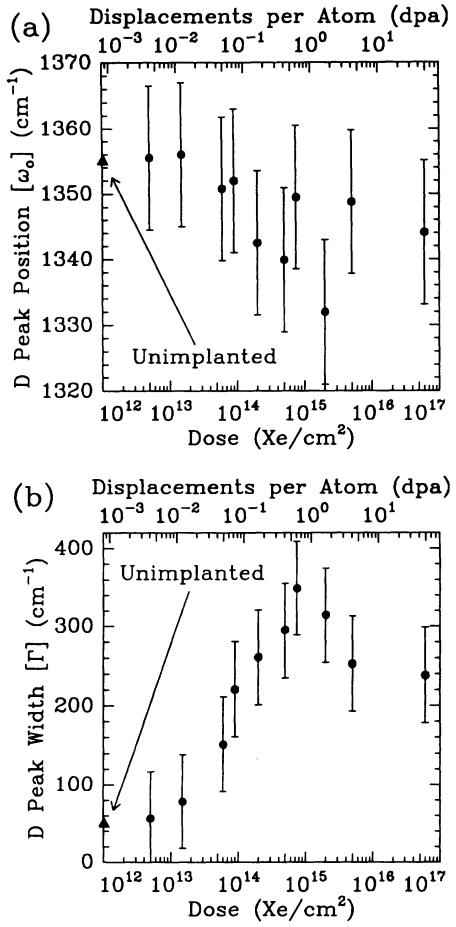

FIG. 5. The (a) position (ω_0) and (b) FWHM (Γ) of the Lorentzian *D* peak plotted against Xe dose. The ▲ on the ordinate axis indicates the values of ω_0 and Γ for unirradiated glassy carbon.

FWHM in Fig. 2(b). Thus the increase in the *D* peak FWHM reflects the introduction of defects into the GC structure which results in an increase in bond-angle disorder.

The picture to emerge from the Raman analysis is then as follows. At damage levels below 0.2 dpa the ion irradiation introduces defects within the essentially intact graphite ribbons of the GC structure. This appears as a broadening of the Raman peaks, and an increase in the *G* peak position and coupling parameter. As the damage level and concentration of defects increase, a reduction in the average size of the graphitic crystallites occurs. At a dpa of ≈ 0.2 the damage level is sufficiently high for the graphitic ribbons to be effectively destroyed. At this point the implanted layer probably contains stable defects such as vacancy and interstitial loops, resulting in bridging and randomization of the basal planes. The downward shift in the *G* peak position which is observed at this damage level suggests that the average bond angle within the irradiated material has been reduced. A reduction in the average bond angle may be accounted for by the presence of five-membered rings which are likely to be present in the highly disordered implanted layer. When the damage level reaches ≈ 1 dpa a saturation of the coupling parameter is observed, suggesting that the structure has been amorphized.

B. High-resolution transmission electron microscopy

Cross-sectional TEM images of the GC specimens implanted at room temperature with 320-keV Xe to doses of (i) 9×10^{13}, (ii) 5×10^{14}, and (iii) 5×10^{15} Xe/cm^2 are shown in Fig. 6. A comparison between unimplanted and implanted areas of the 9×10^{13} and 5×10^{14} Xe/cm^2 samples are shown at a higher magnification in Fig. 7. For the 9×10^{13} Xe/cm^2 sample [Fig. 6(i)], there is evidence that the ion beam has disrupted the GC structure to a depth of approximately 120 nm. However, at higher magnifications the (002) graphitic fringes can still be seen, indicating that at this ion dose the Xe irradiation has not entirely destroyed the tangled graphitic microstructure [Fig. 7(i)]. The image from the 5×10^{14} Xe/cm^2 sample [Fig. 6(ii)] is dominated by the gold surface layer (black band on the right of the image) approximately 20 nm thick. Below the gold layer is a region approximately 130 nm thick in which the tangled graphitic structure is absent [Fig. 7(ii)]. Thus at this Xe dose, which corresponds to a damage levels of 0.4 dpa, the ion bombardment has

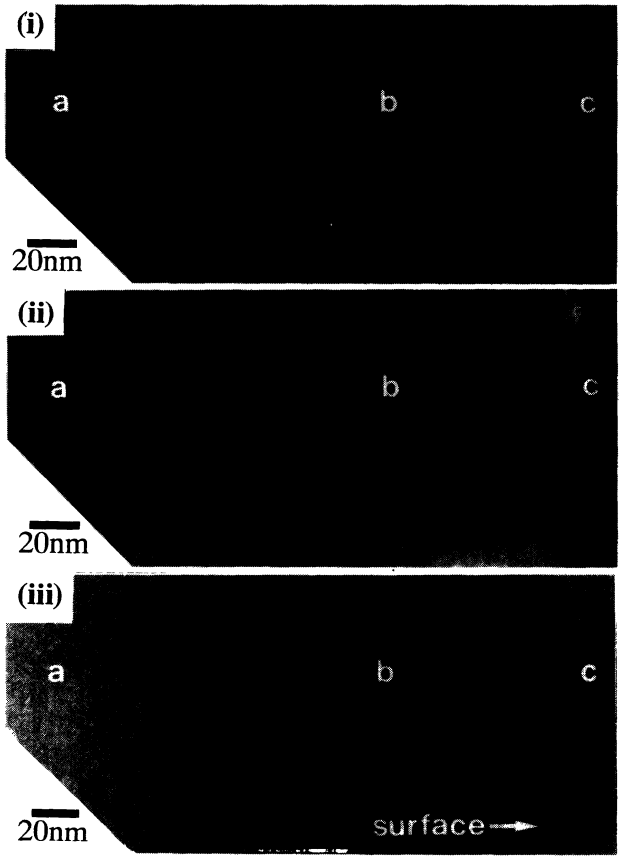

FIG. 6. High-resolution transmission electron microscope images of glassy carbon implanted with 320-keV Xe ions to doses of (i) 9×10^{13}, (ii) 5×10^{14}, (iii) 5×10^{15} Xe/cm^2 prepared in cross section by ultramicrotomy. Region *a* is as-grown glassy carbon, region *b* is the ion-beam-modified layer, and region *c* is a gold surface layer in (i) and (ii) and epoxy resin in (iii).

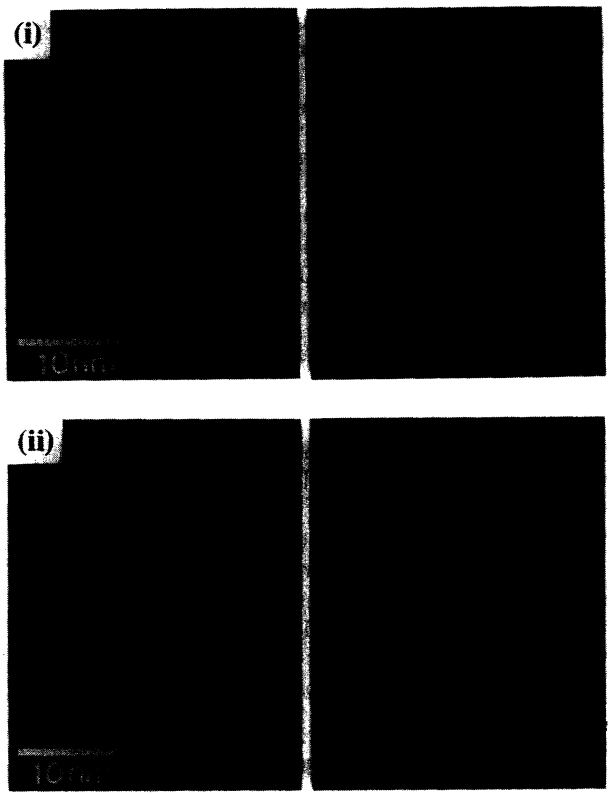

FIG. 7. Comparison between the *a* unimplanted and *b* implanted regions of the glassy carbon samples implanted with (i) 9×10^{13} and (ii) 5×10^{14} Xe-/cm^2 shown at higher magnifications than in Fig. 6.

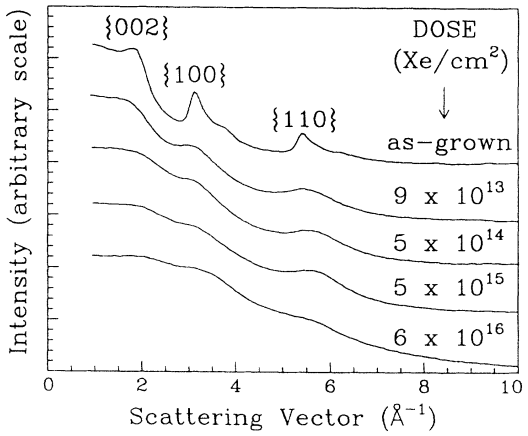

FIG. 8. Plots of radially averaged pixel intensities taken from selected area diffraction patterns of as-grown glassy carbon and the ion-beam-implanted glassy carbon layers of the Xe-implanted samples shown in Fig. 6.

significantly reduced the medium- to long-range graphitic order of the GC structure, as indicated by the absence of the graphitic fringes.

The image from the 5×10^{15} Xe/cm^2 sample [Fig. 6(iii)] is similar to that obtained from GC implanted with 50-keV C to a dose of 5×10^{16} C/cm^2.[18] An amorphous layer can be seen extending from the surface to a depth of 150 nm (region b). In order to create an amorphous surface layer, it is expected that a much lower dose of 320-keV Xe irradiation is required compared to 50-keV C irradiation, since TRIM[21] calculations predict that 320-keV Xe ions create $\approx$ ten times greater lattice damage than 50-keV C ions in GC.

In order to obtain a more sensitive measure of the effects of the ion implantation on microstructure within the implanted layer, selected area diffraction patterns were taken from the implanted layers of the Xe-irradiated samples. The implanted layer was taken to be within the first $\approx$100 nm from the surface of each sample. Care was taken not to include contributions from the gold surface layers or the underlying GC substrate in these diffraction patterns. The resulting ring patterns were digitized using a charge couple device (CCD) camera. Radially averaged pixel intensities were then calculated from the digitized images and plotted in Fig. 8. Also shown for comparison is the digitized diffraction pattern from unirradiated GC. It can be seen from the figure that the irradiation has had a dramatic effect on the diffraction pattern of GC. At a Xe dose of 9×10^{13} ions/cm^2 (corresponding to 0.07 dpa) the {100} and {110} rings have broadened. Also evident is a slight broadening of the {002} ring, suggesting that some disruption of the interplanar bonding has also occurred. However, it is clear from the image of the implanted layer of this sample that the tangled (002) graphitic fringes are still present [Fig. 7(i)], which suggests that the damage at this ion dose is insufficient to destroy the graphitic bonding completely within the implanted layer. Thus this TEM result is consistent with the findings from the Raman spectroscopy study which showed that for a dose of 9×10^{13} ions/cm^2 short-range graphitelike bonding is dominant in the implanted layer.

The rings broaden further for a Xe dose of 5×10^{14} ions/cm^2 (0.4 dpa). In the images of the implanted layer of this sample, the (002) graphitic fringes are no longer present, indicating that the graphitic ribbons of the GC structure have broken up. The diffraction pattern from the 5×10^{15} Xe/cm^2 sample shows broad halos characteristic of those found from *a*-C. Thus at this ion dose, which corresponds to 4 dpa, the ion bombardment has completely amorphized the GC structure. This result is consistent with the saturation observed in the Raman coupling parameter (which is a measure of graphitic order) above $\approx$1 dpa which is also attributed to the formation of an amorphous surface layer.

C. Electron-energy-loss spectroscopy

In order to understand more about the nature of the bonding in the implanted regions, EEL spectra were taken from the GC samples implanted with 320-keV Xe. In Figs. 9(c)–9(e) typical EEL spectra in the low-loss region for GC irradiated with 9×10^{13}, 5×10^{14}, and 5×10^{15} Xe/cm^2 are shown. These spectra were taken with the electron beam positioned in the center of the implanted layer. For comparison purposes, spectra were also obtained from samples of unirradiated GC [Fig. 9(b)], single-crystal graphite (highly oriented pyrolytic graph-

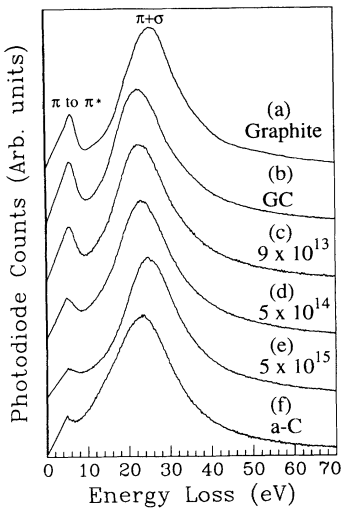

FIG. 9. Electron-energy-loss spectra in the low-loss region of (a) single-crystal graphite, (b) unimplanted glassy carbon, (c)–(e) glassy carbon irradiated with 320-keV Xe to doses of 9×10^{13}, 5×10^{14}, and 5×10^{15} ions/cm^2, and (f) evaporated amorphous carbon (a-C).

ite) [Fig. 9(a)], and evaporated a-C (in the form of a holey carbon film obtained from Agar Scientific Ltd.) [Fig. 9(f)]. All spectra were deconvoluted to give the single scattering component using the Fourier-log method.[27] The zero-loss peaks have also been removed by fitting a symmetric zero-loss peak to the negative-energy tail in each of the spectra. Both these processes were carried out using the Gatan EL/P software (version 2.1).

The dominant feature of all the spectra shown in Fig. 9 is the broad $\pi+\sigma$ plasmon peak at energy losses of between 22 and 26 eV. Also present is a peak between 5 and 6 eV which corresponds to transitions between π and π^* states in graphite. Due to the relatively poor energy resolution of these spectra (1.2 eV), this peak overlaps with the tail of the zero-loss peak, making the determination of its exact position and amplitude difficult. Thus this peak provides qualitative information only. As one would expect, the π to π^* peak of GC is quite intense and has a magnitude similar to that obtained from graphite, reflecting the graphitic nature of the bonding in GC. As the irradition dose is increased, the π to π^* peak is seen to reduce in intensity and broaden, which may indicate a decrease in the ratio of sp^2- to sp^3-bonded carbon atoms. After irradiation at the highest dose, the π to π^* peak is approximately the same intensity as the evaporated a-C [Fig. 9(f)].

The $\pi+\sigma$ plasmon peak positions for each of the samples examined are listed in Table I. The value listed in the table is the average of at least six measurements of the samples analyzed. The largest standard deviation from any set of measurements was 0.2 eV. The $\pi+\sigma$ plasmon peak position for graphite occurs at an energy loss of 25.6±0.2 eV, which is considerably greater than the 22.7±0.2 eV found for unirradiated GC. The lower value for as-grown GC can be explained to some extent by a lower density of electrons contributing to the resonance, which is understandable in terms of the difference

TABLE I. Summary of some important parameters determined from electron-energy-loss measurements for the various materials studied.

Material	Plasmon peak (eV)	sp^2 fraction f
Graphite	25.6±0.2	1.00
Glassy carbon	22.7±0.2	1.00
Glassy carbon irradiated with 9×10^{13} Xe/cm^2	23.1±0.2	1.00±0.05
Glassy carbon irradiated with 5×10^{14} Xe/cm^2	23.6±0.2	1.00±0.05
Glassy carbon irradiated with 5×10^{15} Xe/cm^2	25.1±0.2	0.85±0.05
Evaporated amorphous carbon (a-C)	23.2±0.2	0.85±0.05

in density between GC and graphite (1.55 and 2.27 g/cm^3, respectively). The $\pi+\sigma$ plasmon peak position for the implanted GC is seen to rise with increasing Xe dose, reaching a value of 25.2±0.2 eV for a dose of 5×10^{15} Xe/cm^2. This shift in energy loss indicates that the ion irradiation leads to the formation of an amorphous surface layer with increased electron density. The evaporated a-C was found to have a plasmon peak at an energy loss of 23.2±0.2 eV. It is important to note that, whilst ion bombardment has amorphized the GC structure, the electron density of the implanted material is considerably higher than that found in evaporated a-C.

The electron-energy-loss spectra in the carbon K edge for graphite, unimplanted GC, the Xe-implanted GC samples, and evaporated a-C are shown in Figs. 10(a)–10(f). The background was subtracted from the spectra by fitting a power-law curve and then the spectra were deconvoluted using the Fourier ratio method.[27] The main features in these spectra are the 1s to π^* peak at ≈285 eV and the large broad peak mainly due to 1s to

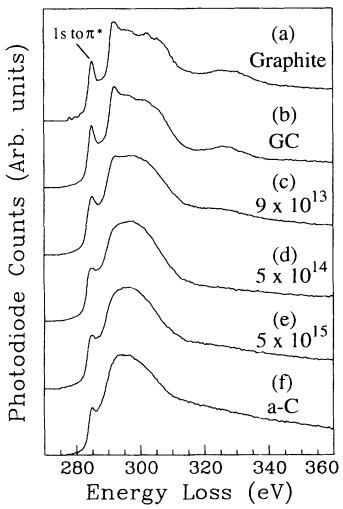

FIG. 10. Background-subtracted electron-energy-loss spectra in the carbon K edge region from (a) single-crystal graphite, (b) unimplanted glassy carbon, (c)–(e) glassy carbon irradiated with 320-keV Xe to doses of 9×10^{13}, 5×10^{14}, and 5×10^{15} ions/cm^2, and (f) evaporated amorphous carbon (a-C).

σ^* transitions at around 300 eV. The 1s to σ^* peaks of the graphite and unimplanted GC samples show a near-edge fine structure which reflects the density of states of the conduction band of grpahite.[28] As the irradiation dose is increased, the spectra show a "washing out" of this fine structure until the spectra become similar to that obtained from the evaporated a-C sample [Fig. 10(f)]. Also evident in Fig. 10 is an apparent decrease in intensity of the 1s to π^* peak for the evaporated a-C film and implanted GC in comparison to graphite and GC. This apparent decrease in the 1s to π^* peak provides good quantitative evidence for a reduction in the proportion of carbon atoms bonded in the graphitelike (sp^2) configuration.

Berger, McKenzie, and Martin[20] have developed a procedure for determining the fraction of sp^2 bonded carbon atoms in carbon materials. This method is based on a comparison of the contribution of the 1s to π^* peak in the carbon K edge to that of a fully graphitized carbon which is taken as a 100% sp^2-bonded reference material.[20] In this calculation the fraction of sp^2 bonds present (f) is calculated using

$$f=\frac{sp^2}{sp^2+sp^3}=\frac{I_{u\pi^*}}{I_{g\pi^*}}\frac{I_g(\Delta E)}{I_u(\Delta E)}\ , \tag{2}$$

where $I_{g\pi^*}$ and $I_{u\pi^*}$ are the integrals from the leading edge to the peak of the 1s to π^* peak of the graphitized and unknown carbon, respectively, and $I_g(\Delta E)$ and $I_u(\Delta E)$ are the integrals over some energy window ΔE of the graphitized and unknown carbon, respectively, which are included in order to normalize K edges collected from the different specimens. The factors $\exp(t/\lambda)$ which are normally applied to Eq. (2) to correct for multiple scattering were not included in this case since the spectra in Fig. 10 have been deconvoluted to give the single scattering component.

Since the intensity of the 1s to π^* peak for single-crystal graphite depends on the beam-to-crystal orientation and other experimental parameters,[20] the $I_{g\pi^*}$ used to calculate the fraction of sp^2-bonded carbon atoms in Eq. (2) was not measured from the graphite sample. Instead, $I_{g\pi^*}$ was measured from unimplanted portions of each of the irradiated GC specimens. This procedure is justified because unimplanted GC microstructurally approximates graphite with randomly orientated crystallites over the area being illuminated by the electron probe. The normalization window was taken to be the integral under the first 100 eV of the carbon K edge.

The fraction of carbon atoms in the implanted layer bonded in the sp^2 configuration (f), evaluated using Eq. (2) for each of the implanted GC samples, is shown in Table I. The values for f are the average from at least six measurements from each of the samples analyzed. The uncertainty in the values of f was taken to be the largest standard deviation from any set of measurements (± 0.05). The relatively large standard deviation is a result of the relatively poor energy resolution of these EEL spectra, which introduces errors due to the overlap of the π and σ peaks. It was found that $f=1.00\pm 0.05$ for the GC samples irradiated to doses of 9×10^{13} and 5×10^{14} Xe/cm^2. This indicates that, although ion irradiation has introduced a significant amount of damage into the GC structure as indicated by the washing out of the near-edge fine structure, the carbon atoms within the implanted material are still bonded predominantly in the sp^2 configuration. For doses up to 5×10^{14} Xe/cm^2 (0.4 dpa), $f=1.00\pm 0.05$ and this is consistent with the Raman results which also suggested that graphitic bonding persists within the implanted layer for damage levels up to ≈ 0.2 dpa. For the 5×10^{15} Xe/cm^2 sample f was found to be 0.85 ± 0.05. Thus, in addition to producing a dense amorphous layer, ion implantation has converted $\approx 15\%$ of the sp^2 bonds into sp^3 bonds at these damage levels. In the case of the evaporated a-C film, f was also measured to be 0.85 ± 0.05.

The conversion of $\approx 15\%$ of the sp^2 to sp^3 bonds in GC under the influence of the ion beam can be explained to some extent by the amorphization of the GC structure. As the ion dose increases and the graphitic ribbons of GC break down and bond-angle disorder increases, it is highly likely that some sp^3 bonds are formed. However, it is important to note that, although the irradiated layer contains a similar fraction of sp^3 bonds as the evaporated a-C (about 15%), the position of the plasmon peak for evaporated a-C was ≈ 23.2 eV, which is substantially less than the plasmon peak position of the GC sample implanted to a dose of 5×10^{15} ions/cm^2 (≈ 25.2 eV). Since the implanted layer has a similar fraction of sp^2 bonding as the evaporated a-C, one may expect the plasmon peak energies for this implanted sample and the a-C to scale as the square root of their densities (i.e., $E_{a\text{-}C}/E_{GC}=\sqrt{\rho_{a\text{-}C}}/\sqrt{\rho_{GC}}$).[27] Using this expression, the density of the implanted sample is calculated to be $\approx 20\%$ higher than the density of the evaporated a-C film. It is clear from this comparison that, although both have a similar fraction of sp^2 bonding, the implanted layer in GC irradiated to a dose of 5×10^{15} ions/cm^2 has a significantly higher density and thus has a more compacted structure than the evaporated a-C film.

D. Ion beam induced compaction

The step heights between implanted and unimplanted regions of the GC samples irradiated at room temperature with 320-keV Xe ions measured using a profilometer are listed in Table II. The trend in the step-height measurements provides evidence against the proposition that ion sputtering has created the measured step. If sputtering were indeed responsible for the observed step then its height would be expected to increase with ion dose. This is not the case, with the step height saturating for doses above 7×10^{14} ions/cm^2. Also listed in Table II are the thicknesses of the implanted layers for the 9×10^{13}, 5×10^{14}, and 5×10^{15} samples, which were measured directly from the cross-sectional TEM images. For the 2×10^{14}, 7×10^{14}, and 2×10^{15} Xe/cm^2 samples the thicknesses were estimated by averaging the measured thicknesses from the next lower and higher dose. As can be seen from the table, no step could be detected to within the extent of surface roughness (± 5 nm) for Xe

TABLE II. The thickness of the amorphous surface layer, step height between implanted and unimplanted glassy carbon regions, and the calculated density for each of the 320-keV Xe-implanted samples.

Xe dose (ions/cm^2)	Thickness of damaged layer (nm)	Step height (nm)	Density (g/cm^3)
9×10^{13}	120±5[a]	0±5	1.6±0.1
2×10^{14}	125±5[b]	0±5	1.6±0.1
5×10^{14}	130±5[a]	30±5	1.9±0.1
7×10^{14}	140±5[b]	50±5	2.1±0.1
2×10^{15}	140±5[b]	60±5	2.2±0.1
5×10^{15}	150±5[a]	60±5	2.2±0.1
6×10^{16}	220±5[a]	c	c
Unimplanted			1.55

[a]Thickness measured from cross-section TEM images.
[b]Thickness was estimated by averaging the measured thicknesses from the next lower and higher dose.
[c]No reliable step could be measured on this sample due to surface blisters (Ref. 7).

doses below 5×10^{14} Xe/cm^2. For Xe doses of 5×10^{14} Xe/cm^2 and above, where a step was measured, the density of the implanted layer was calculated using a simple compaction model[18,29] and plotted in Fig. 11. The density of the implanted layer was found to rise from the as-grown value of 1.5 to 2.2±0.1 g/cm^3 for ion doses above 7×10^{14} Xe/cm^2. This value for the density of the ion-beam-compacted material measured using step heights compares favorably to the estimates for the density based on Rutherford backscattering measurements.[19]

However, the saturation density for the implanted layer of 2.2±0.2 g/cm^3 for Xe doses above 7×10^{14} Xe/cm^2 is somewhat lower than the density of 2.4±0.2 g/cm^3 found previously for the 50-keV C implant for a dose of 5×10^{16} C/cm^2.[18] This discrepancy may be due to the difference in implantation temperature between the C and Xe implants. The C implantation was performed whilst holding the target at ≈150 K while the Xe implantation

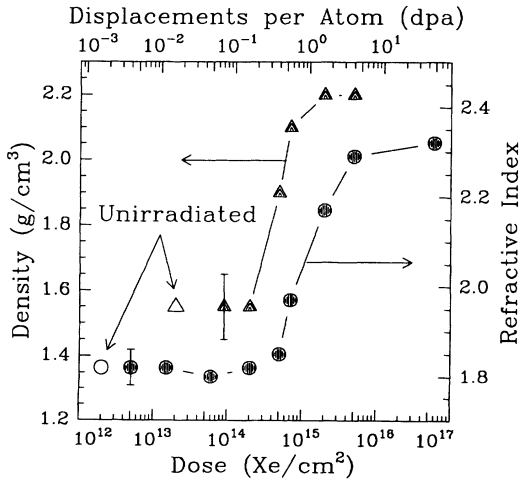

FIG. 11. Density (▲) and refractive index (●) of 320-keV Xe-implanted glassy carbon samples plotted against ion dose (bottom axis) and dpa (top axis).

was performed at room temperature. Raman analysis has revealed differences between samples implanted at room temperature and those implanted at lower temperatures, indicating that dynamic annealing has an important effect on the structure of the implanted layer.[30] The effect of implantation temperature on the structure of implanted GC will be the subject of a forthcoming publication.[31]

Interestingly, it has been shown that the amorphous surface layer produced following the ion implantation of graphite causes the implanted layer to swell, indicating that the density of the implanted layer is considerably less than the density of crystalline graphite (2.26 g/cm^3).[32] Therefore the saturation density of the implanted layer in GC (2.2 g/cm^3) is likely to be considerably higher than that that of the implanted layer in graphite. One possible explanation for this difference in density between an implanted layer in GC and that in graphite is the presence of cross linking between the graphitic ribbons in the GC structure. These interribbon bonds provide stability which keeps the structure from swelling as the damage level increases and the structure amorphizes. The result is an implanted layer in GC which has a higher density than that found in implanted graphite.

Also shown in Fig. 11 is the dose dependence of the refractive index (as determined from ellipsometric measurements) of the GC samples following irradiation with 320-keV Xe ions. It can be seen from this figure that the Xe implantation leads to an increase in the refractive index which saturates at a value of ≈2.3 for ion doses above 5×10^{15} Xe/cm^2. Due to the anisotropic nature of the bonding in graphite, the refractive index varies substantially with the orientation of the graphite crystal. At 546.1 nm, the refractive index of graphite has been measured in the basal plane to be 2.15, compared to 1.81 along the c axis.[33] Since GC is an isotropic graphitic material, one would expect it to have a refractive index somewhere between 1.81 and 2.15. The measured value of 1.8±0.05 for as-grown GC is close to the expected lower limit. The lower value can be explained by the lower density of GC compared to that of graphite. Thus the refractive index of implanted GC is significantly higher than that expected from graphite. The dose dependence of the density mirrors the dose dependence of the refractive index, strongly suggesting that the increase in refractive index is a result of an increase in electron density.

The onset for compaction occurs at a Xe dose of 5×10^{14} ions/cm^2 (0.2 dpa) which is the dose at which the (002) graphitic fringes could no longer be observed in the TEM image of the implanted layer (Fig. 7). A dpa of 0.2 also corresponds to the damage level where the transition between a micropolycrystalline graphite and an a-C was observed in the Raman analysis. Thus the onset of compaction is concomitant with the breakdown of the graphitic ribbons of the GC structure at damage levels above 0.2 dpa.

To some degree, the compaction of the implanted layer in GC can be explained in view of the porous nature of the GC structure. A denser implanted layer could be produced by the filling up of pores as the ion beam breaks

up some of the ribbons in the GC structure into smaller crystallites. The EEL measurements show a shift up in the plasmon energy for irradiated GC consistent with a compacted implanted layer. In addition, since the plasmon peak energy is related to the electron density of the material, these EEL measurements indicate that at least some of the compaction is on an atomic scale and not simply the removal of voids. The EEL measurements also show that ion irradiation leads to the conversion of some of the sp^2 bonds to sp^3. Thus the EEL measurements suggest that, in addition to compaction generated by the filling up of pores by smaller crystallites, the conversion of $\approx 15\%$ of sp^2 to sp^3 bonds in the implanted layer also contributes to the compaction of the implanted layer in GC. The formation of *a*-C materials with densities comparable with graphite and containing local sp^3 bonding has been widely reported.[34,35]

E. Model for improved wear resistance

The threshold and saturation dpa for improved wear resistance in GC implanted with He, C, N, O, F, and Ne ions are approximately 0.1 and 0.5, respectively.[6] The compaction of the implanted layer in GC from 1.55 to 2.2 g/cm^3 occurs at ≈ 0.2 dpa, which is similar to the dpa for the onset in wear resistance. Thus the densification of the implanted layer is likely to be an important factor in contributing to the observed increase in wear resistance. As it is well known that the GC structure contains voids or pores and porosity has been identified as a source of mechanical weakness in GC, it is reasonable to suppose that a reduction in porosity would greatly strengthen the material by suppressing crack propagation. In addition to a reduction in pore size, the presence of $\approx 15\%$ sp^3 bonding in the implanted material probably also contributes to the overall toughness of the ion-beam-modified layer. a-C films of exceptional strength have been produced by various techniques such as ion-beam and plasma deposition.[34,35] We propose that ion implantation of GC to damage levels about 0.2 dpa produces a material with a structure similar to some of these hard carbon films. The structural properties of the implanted material are as follows: relatively high volume density of ≈ 2.2 g/cm^3, a high degree of bonding disorder, and the presence of $\approx 15\%$ sp^3 bonding. Thus the increase in wear resistance observed in implanted GC can be explained by the formation of a hard, compacted *a*-C surface layer following ion irradiation to damage levels above 0.2 dpa.

Finally, we note recent models for the structure of hard or diamondlike carbon films prepared by filtered, vacuum arc deposition. These sp^3-bonded films are thought to be stabilized by the compressive stress generated by the shallow implantation of carbon ions.[34,36] Since it has been shown by us that the implanted layer in GC is significantly compacted, it is reasonable to assume that this layer may also be under considerable compressive stress. This stress may also be a source of toughening, as a compressive stress would tend to suppress crack propagation and lead to a more wear-resistant layer. Stress measurements on implanted GC have not been carried out to date to our knowledge, but we intend to conduct such measurements on the implanted layer in GC to test this possibility.

IV. CONCLUSION

A detailed investigation of the transformation which occurs in GC following ion implantation has been presented. It was found that the ion-beam-induced transformation occurs in two stages. At low damage levels (<0.2 dpa) the GC structure maintains its graphitic microstructure but displays a reduction in the average graphitic crystallite size as defects are introduced by the ion beam. Above 0.2 dpa, the implanted material begins to transform from one with a graphitic microstructure to one in which even the local bonding is not strictly threefold coordinated. During amorphization $\approx 15\%$ of the graphitelike bonds are converted into diamondlike bonds and the density of the implanted layer increases from 1.55 to ≈ 2.2 g/cm^3. The structure of the amorphous implanted layer differs from that of evaporated *a*-C and is more like the "hard" carbon films produced by ion-beam or plasma deposition techniques. The increase in wear resistance observed in implanted GC can be attributed to the formation of this hard, compact, amorphous carbon surface layer at damage levels above 0.2 dpa.

ACKNOWLEDGMENTS

This work is supported by a grant from the Australian Research Council. The authors wish to thank Alex Moodie at the Department of Applied Physics, RMIT for his assistance with the TEM measurements and Rafi Kalish and Vova Richter at the Technion, Israel for implanting some of the GC samples which appear in this work. Rafi Kalish is also thanked for many helpful suggestions on this manuscript.

*Present address: Electron Microscope Unit, University of Sydney, NSW 2006, Australia.

[1]M. S. Dresselhaus and R. Kalish, *Ion Implantation in Diamond, Graphite and Related Materials* (Springer-Verlag, Berlin, 1992).

[2]G. M. Jenkins and K. Kawamura, *Polymeric Carbons-Carbon Fibre Glass and Char* (Cambridge University, Cambridge, England, 1976).

[3]J. S. Williams, Rep. Prog. Phys. **49**, 491 (1986).

[4]K. Yoshida, K. Takahashi, K. Okuno, G. Katagiri, M. Iwaki, and A. Ishitani, Appl. Phys. Lett. **52**, 1046 (1988).

[5]M. J. Kenny, J. T. A. Pollock, and L. S. Wielunski, Nucl. Instrum. Methods Phys. Res. Sect. B **39**, 704 (1989).

[6]J. T. A. Pollock, M. J. Kenny, L. S. Wielunski, and M. D. Scott, in *Structure-Property Relationships in Surface-Modified Ceramics*, Vol. 170 of *NATO Advanced Study Institute, Series E: Applied Sciences*, edited by C. J. McHargue, R. Kossowsky, and W. O. Hofer (Kluwer Academic Publishers, Dordrecht, 1989), p. 321.

[7]D. McCulloch and S. Prawer, J. Comput. Aided Microsc. **4**, 281 (1993).

[8]D. S. Knight and W. B. White, J. Mater. Res. **4**, 385 (1989).

[9]R. Al-Jishi and G. Dresselhaus, Phys. Rev. B **26**, 4514 (1982).
[10]K. Yoshida, K. Okuno, G. Katagiri, A. Ishitani, K. Takahashi, and M. Iwaki, in *Fundamentals of Beam-Solid Interactions and Transient Thermal Processing,* edited by M. J. Aziz, L. E. Rehn, and B. Stritzker, MRS Symposia Proceedings No. 100 (Materials Research Society, Pittsburgh, 1988), p. 207.
[11]S. Prawer, F. Ninio, and I. Blanchonette, J. Appl. Phys. **68**, 2361 (1990).
[12]R. O. Dillon, J. A. Woollam, and V. Katkanant, Phys. Rev. B **29**, 3482 (1984).
[13]M. V. Klein, in *Light Scattering in Solids I,* edited by M. Cardona, Topics in Applied Physics Vol. 8 (Springer-Verlag, Berlin, 1975), p. 147.
[14]B. S. Elman, M. S. Dresselhaus, G. Dresselhaus, E. W. Maby, and H. Mazurek, Phys. Rev. B **24**, 1027 (1981).
[15]B. S. Elman, M. Shayegan, M. S. Dresselhaus, H. Mazurek, and G. Dresselhaus, Phys. Rev. B **24**, 4142 (1982).
[16]M. S. Dresselhaus and G. Dresselhaus, in *Light Scattering in Solids III,* edited by M. Cardona and G. Guntherodt, Topics in Applied Physics, Vol. 51 (Springer-Verlag, Berlin, 1982), p. 3.
[17]D. Beeman, J. Silverman, R. Lynds, and M. R. Anderson, Phys. Rev. B **30**, 870 (1984).
[18]D. McCulloch, A. Hoffman, and S. Prawer, J. Appl. Phys. **74**, 135 (1993).
[19]D. McCulloch, S. Prawer, A. Hoffman, and D. K. Sood, Nucl. Instrum. Methods Phys. Res. Sect. B **80/81**, 1451 (1993).
[20]S. D. Berger, D. R. McKenzie, and P. J. Martin, Philos. Mag. Lett. **57**, 285 (1988).
[21]J. F. Ziegler, J. P. Biersack, and U. Littmark, *The Stopping and Range of ions in Solids* (Pergamon, New York, 1985).
[22]T. F. Malis and D. Steele, in *Specimen Preparation for Transmission Electron Microscopy of Materials II,* edited by R. Anderson, MRS Symposia Proceedings No. 199 (Materials Research Society, Pittsburgh, 1990), p. 3.
[23]R. M. A. Azzam and N. M. Bashara, *Ellipsometry and Polarised Light* (North-Holland, Amsterdam, 1977).
[24]P. Lespade, R. Al-Jishi, and M. S. Dresselhaus, Carbon **20**, 427 (1982).
[25]S. Prawer and C. J. Rossouw, J. Appl. Phys. **63**, 4435 (1988).
[26]F. Tuinstra and J. K. Koenig, J. Chem. Phys. **58**, 1126 (1970).
[27]R. F. Egerton, *Electron Energy Loss Spectroscopy in the Electron Microscope* (Plenum, New York, 1986).
[28]R. F. Egerton and M. J. Whelan, J. Electron Spectrosc. **3**, 232 (1974).
[29]A. Hoffman, P. J. Evans, D. D. Cohen, and P. J. K. Paterson, J. Appl. Phys. **72**, 5687 (1992).
[30]M. Iwaki, K. Takahashi, and A. Seiguchi, J. Mater. Res. **5**, 2562 (1990).
[31]D. G. McCulloch and S. Prawer (unpublished).
[32]J-P. Hirvonen, D. Stone, M. Nastasi, and S-P. Hannula, Scr. Metall. **20**, 649 (1986).
[33]S. Ergun, Nature **213**, 136 (1967).
[34]D. R. McKenzie, D. Muller, and B. A. Pailthorpe, Phys. Rev. Lett. **67**, 773 (1991).
[35]J. Robertson, Adv. Phys. **35**, 317 (1986).
[36]J. Robertson, Diamond Relat. Mater. **2**, 984 (1993).

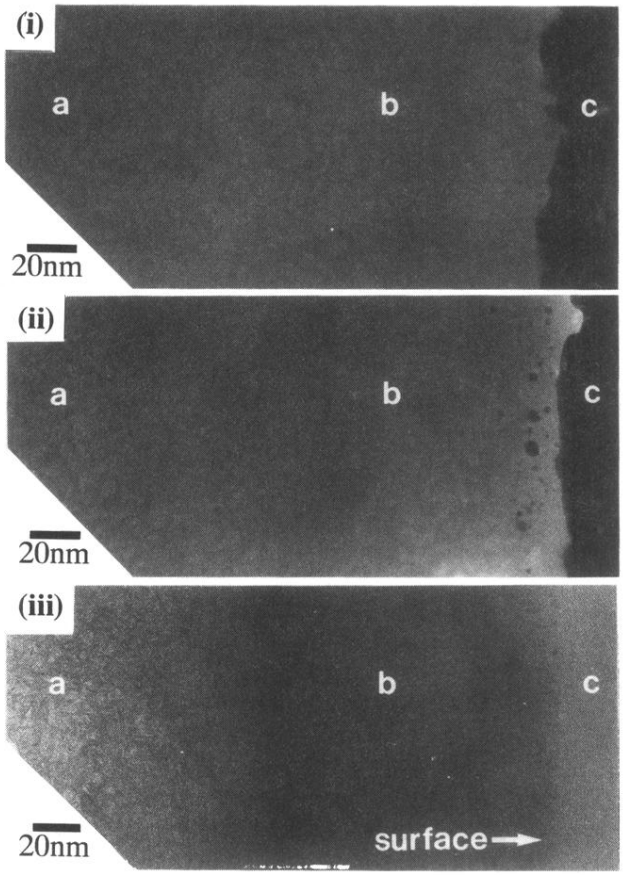

FIG. 6. High-resolution transmission electron microscope images of glassy carbon implanted with 320-keV Xe ions to doses of (i) 9×10^{13}, (ii) 5×10^{14}, (iii) 5×10^{15} Xe/cm^2 prepared in cross section by ultramicrotomy. Region *a* is as-grown glassy carbon, region *b* is the ion-beam-modified layer, and region *c* is a gold surface layer in (i) and (ii) and epoxy resin in (iii).

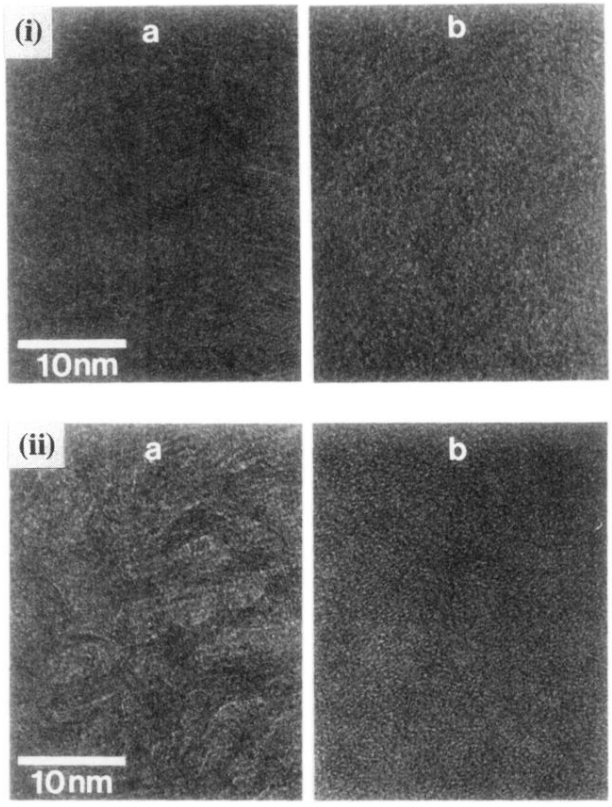

FIG. 7. Comparison between the *a* unimplanted and *b* implanted regions of the glassy carbon samples implanted with (i) 9×10^{13} and (ii) 5×10^{14} Xe-/cm^2 shown at higher magnifications than in Fig. 6.